The Measurement of Shallow Ocean Currents Beneath Deformed Mobile Sea Ice using Upward Looking Sonar Instruments.

Todd D. Mudge
ASL Environmental Sciences Inc.
Victoria, BC, Canada
tmudge@aslenv.com
David B. Fissel, Nikola Milutinovic, Keath Borg, Dawn Sadowy, and Ed Ross
ASL Environmental Sciences Inc.
Victoria, BC, Canada
dfissel@aslenv.com, milni@aslenv.com, kborg@aslenv.com, dsadowy@aslenv.com and eross@aslenv.com.

ABSTRACT
The under ice ocean currents are critical in the understanding of the boundary layer between the sea ice and the ocean, involving determination of the drag forces that sea-ice exerts on the upper water column and the related turbulence and mixing levels. A semi-automated algorithm has been developed, which accounts for the changes in sea ice drafts, to determine the nearest surface ocean current measurement level. Using long-term measurements from upward looking sonar datasets in the Chukchi and Beaufort Seas, the algorithm and its extensions to all current bins is investigated.

KEY WORDS: Sea Ice, Ocean Currents, Boundary Layer, Chukchi Sea, Beaufort Sea.

INTRODUCTION

Ocean Current Measurements Under Ice

The ice covered oceans represent a challenge to the measurement of near surface ocean currents. The presence of ice keels, some that are tens of metres thick, limits the depths in which instruments can be deployed without potential damage. Current measuring instruments have been deployed from the ice surface (McPhee 2013; Mudge 2005); however these are typically of limited duration and, in the case of mobile sea ice, are destined to travel an unplanned path that may not be of interest to the end-user. Over the last two decades, numerous moored Upward Looking Sonars (ULS) have been deployed in Arctic waters to measure ice draft and ocean currents. These deployments have largely been by research groups, such as Department of Fisheries and Oceans Canada (DFO), ArcticNet, Woods Hole Oceanographic Institute and Norwegian Polar Institute, or for oil and gas companies. For oil and gas projects, metocean data regarding the sea ice and oceanographic characteristics are obtained. For measurement of ocean currents, the most difficult to attain are the near-surface currents below the sea ice/water interface. ASL has developed a semi-automated method to extract the currents from as near the sea ice interface as possible.

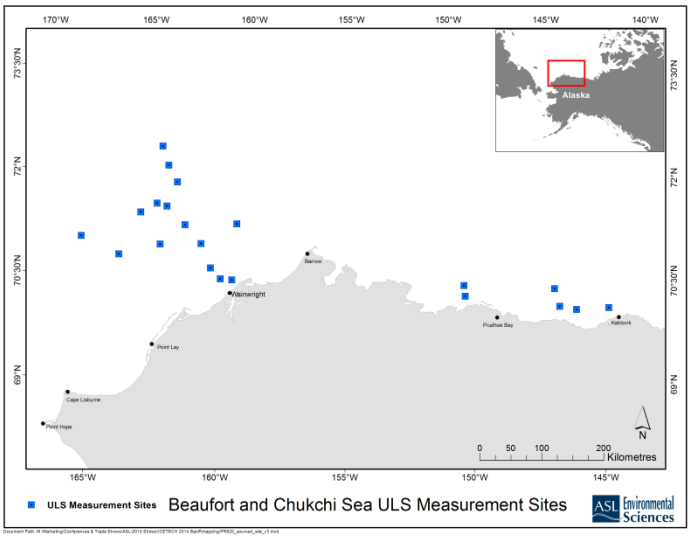

Figure 1. Upward Looking Sonar sites in the Chukchi and Beaufort Seas for Shell, ConocoPhillips and Statoil.

Deployments in the Chukchi and Beaufort Seas

Over the last nine years, ASL has serviced year-long ULS moorings at over 20 sites in the Chukchi and Beaufort Seas for Shell, ConocoPhillips and Statoil (Figure 1). Most of these sites have been instrumented with a combination of a Teledyne RDI Acoustic Doppler Profiler (ADCP) and an ASL Ice Profiling Sonar (IPS) in separate taut-line moorings that are approximately 100 m apart (Figure 2). Data analysis has been primarily focused on providing metocean inputs regarding sea ice and physical oceanographic characteristics for engineering design and operational planning.

From 2005 to 2013, ASL, originally in collaboration with Dr. Humfrey Melling (DFO) and more recently with Olgoonik-Fairweather, has supported one to three concurrent ULS sites in the Beaufort Sea for

Shell. Deployments of four sets of ULS moorings in the Chukchi Sea began in 2008 for Shell and ConocoPhillips in collaboration with DFO and Olgoonik-Fairweather. After 2009, Olgoonik-Fairweather provided the vessels for servicing all ASL operated ULS moorings in the Chukchi and Beaufort Seas. In 2011, Shell, ConocoPhillips and Statoil supported ASL's one year deployment of 6 ADCP moorings in the vicinity of Hanna Shoal in the Chukchi Sea. For the 2012-2013 season, Statoil supported two ULS moorings in the vicinity of their lease blocks. Shell continues to support four sets of ULS moorings in the Chukchi Sea and a single set in the Beaufort Sea. ConocoPhillips and Statoil discontinued their ULS programs in 2013.

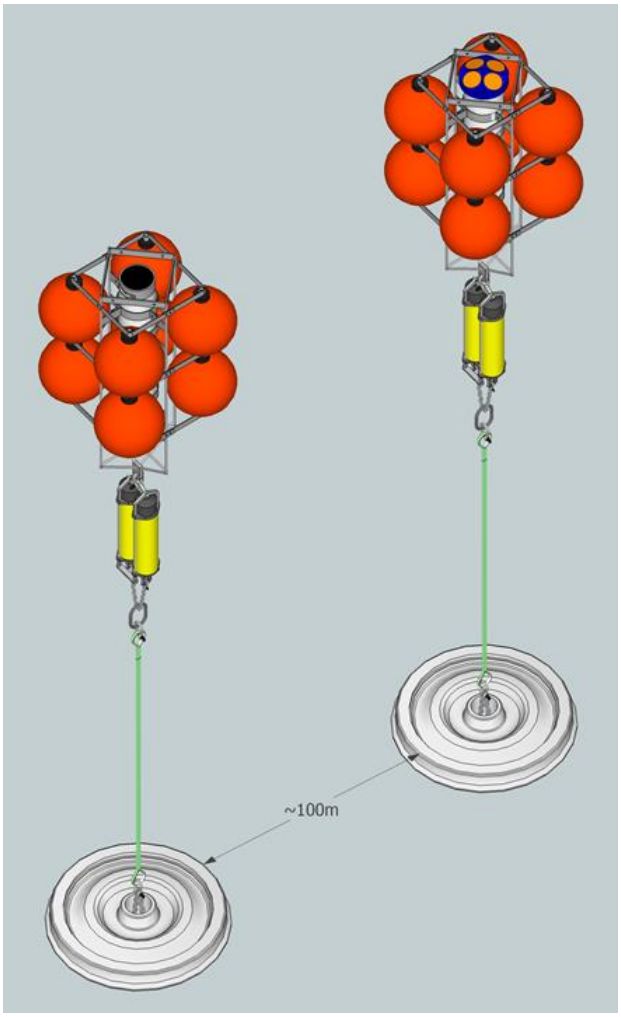

Figure 2. Ice Profiling Sonar (left) and Acoustic Doppler Current Profiler (right) taut-line moorings as deployed in the Chukchi and Beaufort Seas.

UPWARD LOOKING SONARS

Acoustic Doppler Profilers

The sites in the Chukchi and Beaufort Sea have been instrumented with Acoustic Doppler Current Profilers (ADCP), Sentinel Workhorse series, manufactured by Teledyne RD Instruments of Poway, California. Most of the deployments have been with 300 kHz ADCPs though early deployments in the Beaufort Sea were originally with 600 kHz units, but were upgraded due to limited range in the later winter and early spring. The ADCP technology is widely used for oceanic environmental monitoring applications. Mounted near the sea bottom, the ADCP unit provides precise measurements of ocean currents (both the horizontal and vertical components) at levels within the water column, from near surface to near-bottom. In addition, the ADCP provides time series measurements of the velocity of the sea ice moving on the ocean's surface.

The ADCP instruments measure velocity by detecting the Doppler shift in acoustic frequency, arising from water current (or ice) movements, of the backscattered returns of upward (20° from vertical) transmitted acoustic pulses. The Doppler shift of the acoustic signals was used to determine water velocities at a vertical spacing, known as bins, of 2 m for the Chukchi and Beaufort sites. To ensure data returns in winter when there are fewer scatterers in the water column, the ADCPs were configured to operate in narrowband mode with 5 minute sample rates. The Sentinel ADCPs were modified by RDI in 1996 to use the Doppler shift from the ice bottom surface to measure ice velocity and backscatter on each beam to determine the distances to the ice.

Ice Profiling Sonars

The IPS instrument is an upward-looking ice profiling sonar, which provides high-quality ice thickness, or more correctly, ice draft data required for characterizing the winter oceanic environment. Originally, this instrument was designed by the Institute of Ocean Sciences, Victoria, BC, Canada (Melling et al., 1995), and has been further developed and subsequently manufactured by ASL. The ice keel depth is determined from the return travel time of an acoustic pulse (420 kHz; 1.8° beam at -3 dB) reflected off the underside of the sea ice. The return time is converted to an acoustic range value through the use of the speed of sound in seawater.

In the Chukchi and Beaufort Seas programs, the current version of ASL's ice profiler (IPS5; Fissel et al., 2007), was setup to run through various configurations (phases) to acquire the best data based on climatological conditions. Ice phases sampled continuously every 1 or 2 seconds providing better than 1 m horizontal resolution of ice draft during the winter. During shoulder months, 1 Hz sampling provided both continuous ice draft and waves depending upon ice coverage. During the summer months, 2 Hz wave bursts provided non-directional wave data.

ANALYSIS METHODS

Typical analysis of ocean currents as inputs to engineering design starts with the identification of key depths where quality controlled data will be provided. With ADCP data, this is done by selecting bins at set distances away from the instrument. ADCP bins in the mid water column and near the instrument are typically of high quality and are relatively easy to process. The bins near the surface are more difficult to process given the presence of ice keels (Figure 3), large waves or changes in tidal depths.

Teledyne ADCPs with 20° beam angles are limited to how close to the ice or sea surfaces that they can validly acquire ocean currents. The ice and sea surfaces are normally more effective in scattering acoustic energy than the scatterers (particles, plankton, gas bubbles, etc.) in the water column. Though there is only a small amount of acoustic energy that has a direct path from the ADCP transducers to the surface, relative to the main lobe that is oriented 20° off vertical, the backscattered energy from the ice and sea surfaces, called sidelobe contamination, usually dominates the weak backscatter from the water column. This sidelobe contamination reduces the effective range of an ADCP by 6% when the ADCP is pointed at a flat surface. When the surface is not flat, such as in the presence of an ice keel (Figure 3), the four-beam Janus configuration of the ADCP can produce valid along-beam currents at different depths for the individual beams. A minimum of three along-beam currents are necessary to calculate the east, north and

vertical ocean currents. Ideally, all four along-beam currents are available as this produces currents with lower errors and provides an additional quality control check for homogenous flow, known as the error velocity.

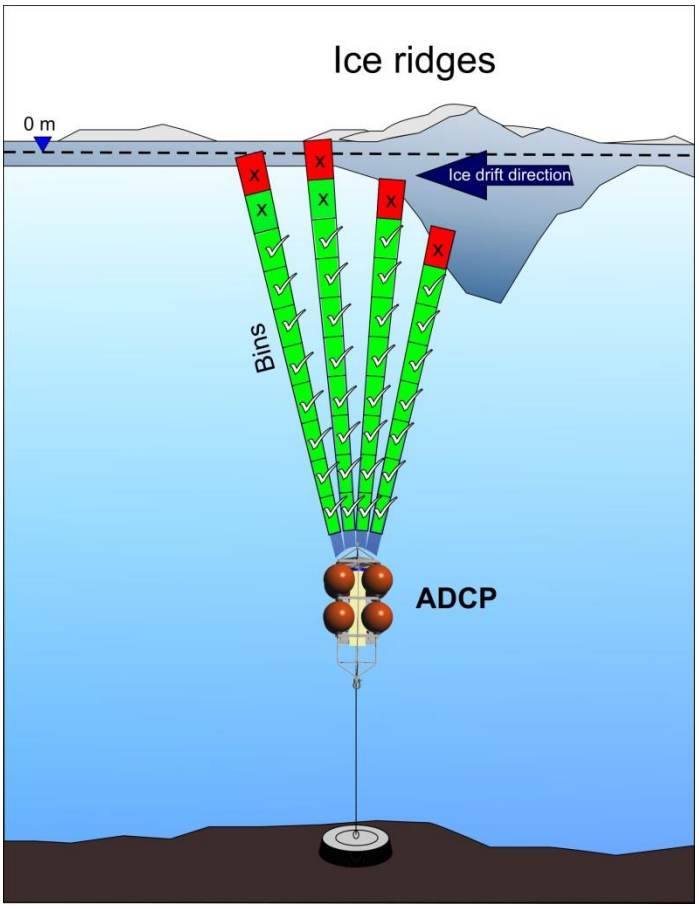

Figure 3. ADCP bins with valid Doppler solutions (green) and valid three or four beam solutions (check marks).

Teledyne RDI ADCP's automatically determine, on a ping by ping basis, the valid three or four beam solutions for each bin. These earth coordinate solutions are ensemble vector averaged into a current profile from typically 10's to 100's of individual water pings to produce currents with approximately 1 cm/s precision. For autonomous deployments, such as those in the Chukchi and Beaufort Seas, the results are internally recorded. To determine the ice velocity, the water pings are intermingled with specialized bottom-tracking pings. Each bottom-tracking ping has a precision of about 0.1 cm/s

Specification of the Near Surface Bin

Following similar techniques used for vessel-based downward-looking ADCPs, ASL has developed a semi-automated algorithm which uses bottom tracking ranges to identify the shallowest valid bin where the water pings have not been contaminated by the presence of ice (Figure 4). This results in an ocean current time series, from the shallowest possible depths, that is based on measured data with only a small amount of rejected or fitted data.

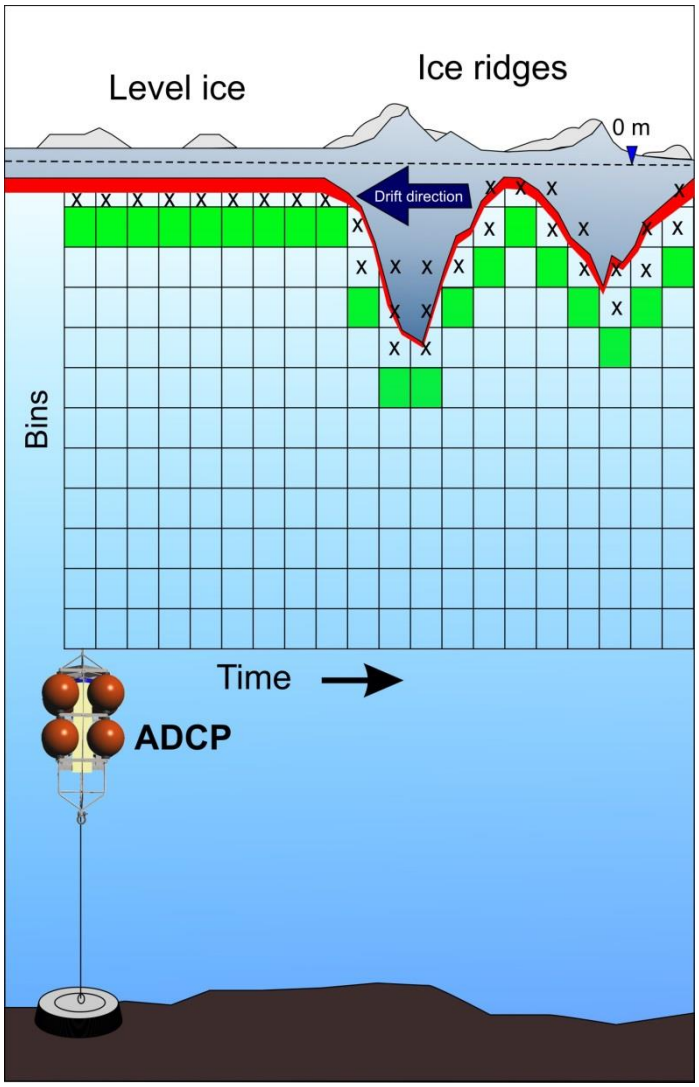

Figure 4. Near surface bin as ice keel drifts past an ADCP.

A significant impediment to this algorithm is the relatively low temporal resolution of the bottom-tracking pings. For most vessel-based systems, pairs of bottom-tracking and water pings are recorded in real-time to an external computer at a rate of up to 1 Hz. Given the storage and power limitations of a taut-line mounted system that is running autonomously for one year, the highest achievable resolution is on the order of minutes. In the case of the Chukchi and Beaufort Sea moorings, most of the instruments collected 5 minute ensembles with 3 bottom pings and about 20 water pings that were evenly distributed in time.

We thus do not have the luxury of cropping each individual water ping profile based on a concurrent bottom-tracking profile. The interleaving of multiple pings during a 5 minute ensemble means that cropping the current profiles in post-processing based on just the bottom tracking ranges within the ensemble will not be 100% effective. Fortunately, the ADCP's false target rejection algorithm calculates a three-beam solution if the intensity from a single beam differs by a significant amount from the other beams. However, if more than one beam's intensity was significantly different from the other values, no measured value is recorded by the ADCP. Due to the possibility of three beam current solutions containing some contamination from the ice, an

assumption was made that if ice was present in one of the beams, but not the other three, the built-in data rejection algorithms of the ADCP would discard the data in the blocked beam, and generate an acceptable solution. Therefore, the third shallowest depth, as detected by the bottom-track pings from each of the four beams, was used as a cutoff for determined the shallowest valid currents.

For periods of open water or partial ice cover, using only the bottom tracking distances is insufficient. The bottom-tracking pings do not consistently detect the sea surface. Thus, the pressure sensor data from the ADCPs is used to determine the instrument depth. Depth was calculated for the Chukchi and Beaufort Sea data sets using the hydrostatic pressure equation Pressure = ρ·g·Depth using a nominal water density, ρ = 1025 kg/m^3, and a nominal acceleration due to gravity, g = 9.8 m/s^2.

An offset to bring the bottom-tracking range and pressure time series derived depth to the same level, in the absence of ice, was selected. A sidelobe correction factor of 0.9397 (cos 20°) was applied to the ranges. An approximation of the significant wave height was found based on the ADCP pressure data. The deeper of the wave height and the sidelobe corrected ranges was chosen, and the bin corresponding to this depth was selected. The time-series of selected bins and currents were examined. In cases where shear in the water column, and changing of bin-number seemed to be creating artifacts in the velocity time series, the selected bin was edited to remove the artifact.

RESULTS

Near Boundary Current Bin

For the Chukchi and Beaufort data sets, ADCP current and ice velocity samples were collected in 5 minute ensembles. The ice velocities had precisions of better than 1 cm/s; however, the currents required further averaging to attain a 1 cm/s precision. Three 5 minute ensembles were averaged together to produce a final 15 minute currents sample. For currents from the mid and near instrument bins, the results were virtually identical to the ADCP being setup to internally average 15 minute bins. For the near surface bin (Figure 4), the averaging of bins from various depths can create unique average bin depths that are in between the standard ADCP bin depths.

The procedure outlined above has been applied to the data from Shell's, ConocoPhillips's and Statoil's data sets. A short two and half day section of current data from the Chukchi Sea (Figure 5) shows the complexity of the near-surface bin. The depth of the ice as detected by the five minute samples of the ADCP (red line, bottom panel) shows significant variability from about 2 m to over 10 m, with the presence of numerous keels. However, as indicated by the ice drafts (blue line, bottom panel) from the 1 Hz sampling IPS unit located approximately 100 m away, the ADCP is likely missing a number of ice keels which travel past the ADCP in between the bottom track pings. To reduce the potential of biasing of the near surface currents due to the inappropriate incorporation of Doppler shifts from the ice, the automated choice of near-surface bin depth (green line, bottom panel) can be made "sticky" by the analyst – the bin will not move up and down on each individual sample but will instead take additional time to respond to changes in ice draft.

The resultant near surface current (red line, top panel of Figure 5), from an ADCP deployed at approximately 45 m water depth, shows a continuous unbiased time record that has not required manual data removal or interpolation over data gaps. The center of the two metre resolution bin has been kept within about 4 m of the ice/water interface as the ice draft varies from 1 m to about 10 m. The speed of the ice drift (blue line, top panel of Figure 5) shows the two speeds are somewhat correlated but they are not identical, indicating the presence of shear and of forcing on the currents from deeper in the water column.

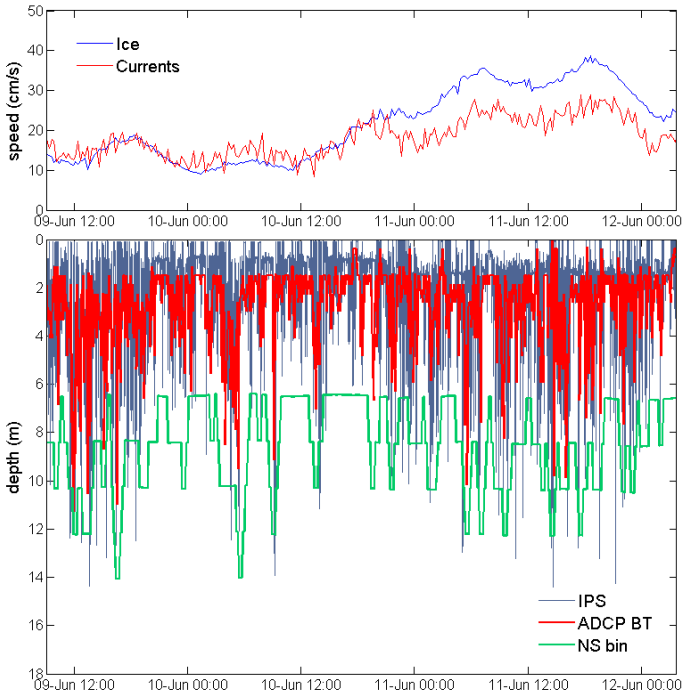

Figure 5. Example section of near surface bin current speed and ice drift speed under a rough ice canopy (top panel). Ice draft as measured by IPS (blue), distance to ice as measured by the ADCP bottom track (red) and resultant near surface bin depth (green) (bottom panel).

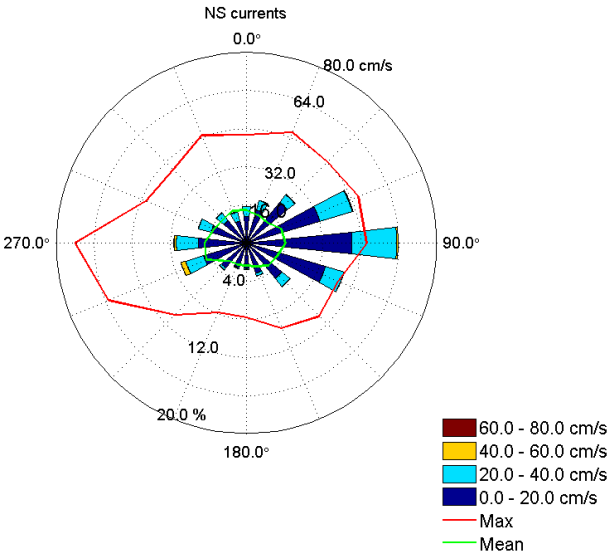

Figure 6. Rose plot for one year of near surface velocities from the Chukchi Sea during the 2012-2013 deployment.

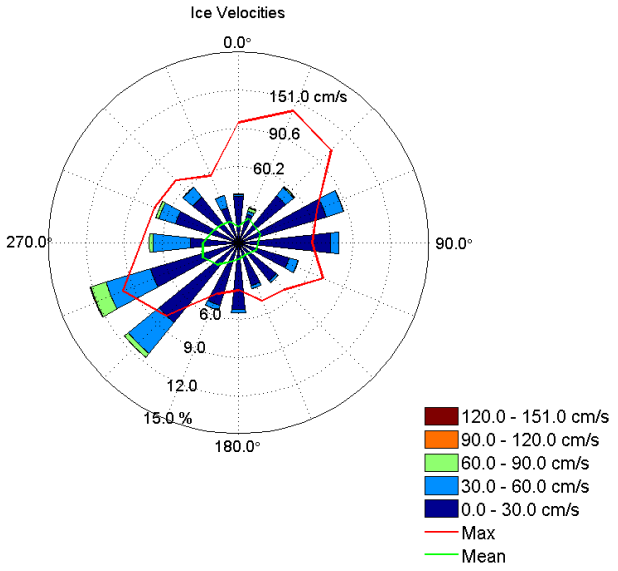

Figure 7. Rose plot of ice velocities for the 2012-2013 ice season in the Chukchi Sea.

The distributions of near surface currents (Figure 6) and the ice drift velocities (Figure 7) for a 2012-2013 deployment in the Chukchi Sea indicate slightly different distributions. The slightly more east-west distribution of the currents in comparison to the more northeast-southwest distribution of the ice velocities is suggestive of the Coriolis Effect, as first observed by Nansen and explained by Ekman (1905). However, care should be taken, as the distribution of the currents includes the open water seasons. What is irrefutable, is the maximum ice velocity speed of 113 cm/s was considerably greater than the near-surface maximum speed of 72 cm/s, thus showing the importance of wind-forcing to produce the highest ice speeds and the presence of considerable velocity shear just below the ice.

Turbulent Boundary Layer

The methodologies and data products developed for the near-surface bins can be further extended. The analysis of all available current bins from ADCPs and not just the nearest to the ice interface can lead to further applications. Examples are shown of how the data might be extended into boundary layer and drag studies.

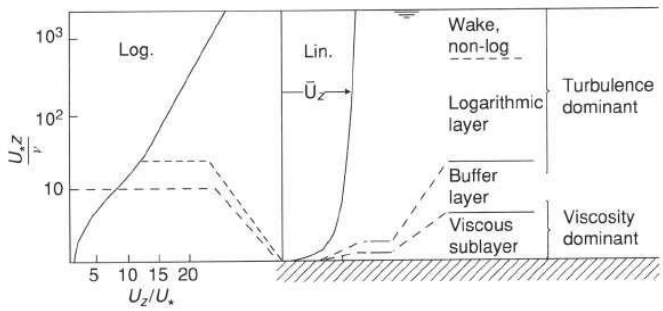

Figure 8. Boundary layer characteristics in a typical near-bottom flow. The vertical axis is logarithmic (Log.) and linear (Lin.) (McCave, 2005)

Studies of near-bottom boundary layers (Lueck and Lu, 1997) show that oceanographic boundary layers can follow the classic law-of-the-wall (Tennekes and Lumley, 1972). The boundary layer currents are characterized by an extremely thin (centimetres) viscous sublayer where viscous stresses dominate. Beyond the viscous sublayer, there is a transition to a region where the mean currents of the flow varies as the natural logarithm of distance from the boundary (z). This turbulent layer's mean current follows.

$$U = u_*/\kappa \cdot ln(z/z_o) \quad (1)$$

where u_* is the friction velocity, κ is the von Kármán's constant (~0.4) and z_o is the roughness length. The roughness length scales at about one thirtieth of the bed roughness (e.g. sand grain diameter for bottom boundary studies). The drag coefficient for the boundary can be determined for some reference height z_r as

$$C_D = (\kappa / ln(z_r/z_o))^2 \quad (2)$$

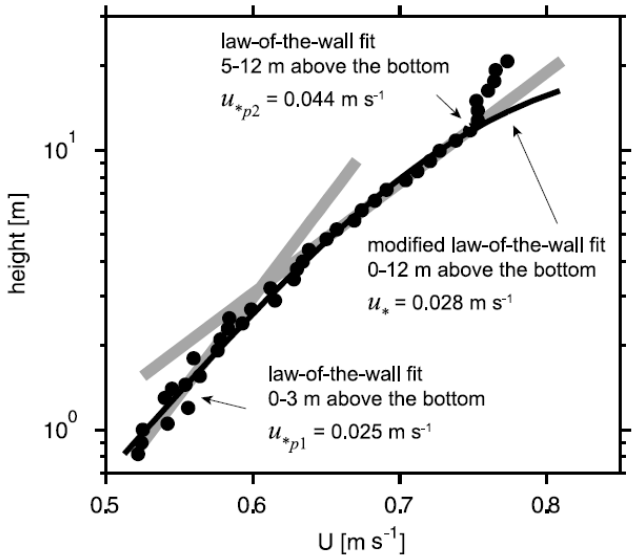

Figure 9. Bottom boundary layer with two logarithmic velocity distributions. Perlin et al. (2005) developed a modified law-of-the-wall for the log-layer further from the boundary that better estimated the frictional velocity.

Unfortunately, the presence of a logarithmic distribution at greater than 5 m away from the ice interface is not conclusive proof that the region is well mixed and that the law-of-the-wall can be directly applied. Perlin at al. (2005) show the well-known presence of two logarithmic distributions in some bottom boundary layers (0-3 m and 5-12 m) can be explained by the presence of stratification in the outer log-layer. This stratification supports a greater velocity shear resulting in an artificially large friction velocity when an unmodified law-of-the-wall is applied. A modified law-of-the-wall was proven to correctly estimate friction velocities (Figure 9). The presence of stratification is less likely to occur early in the ice season due to the extrusion of salt brine associated with the formation of sea ice which effectively mixes the underlying water column to depths of tens of metres. However, in the spring or early summer, stratification is more likely to occur.

Conditions for the development of a turbulent logarithmic boundary layer include

- The forcing is nearly constant. For an ice/water boundary layer this happens when the ice velocity is steady.
- There has to be little stratification or else mixing becomes a sink for the turbulence.
- Turbulence from other sources is weak.

- The turbulent boundary layer dominates the Coriolis force. This scales as a distance, $\kappa \cdot u_* / f$, (f is the Coriolis frequency) from the boundary.

These conditions are most easily achieved near the ice boundary and thus lend themselves to measurements from the ice such as those done by McPhee (2013) and Mudge (2005), where current measurements were completed within 1 m of the ice/water interface by current meters deployed from the ice. To develop a turbulent log layer under the ice that can be resolved by the ADCPs mounted in the taut-line moorings in the Chukchi and Beaufort Seas requires times when the ice velocities are both stable and relatively large. Limiting ourselves to these conditions, there are a number of potential cases to study within the years of data from the Chukchi and Beaufort Seas sites.

One of these cases from November 2012 had ice speeds that were relatively stable at about 50 to 60 cm/s for over 6 hours (Figure 10). The ice generated currents of about 30 cm/s near the surface; there is an apparent shear as currents decrease with depth.

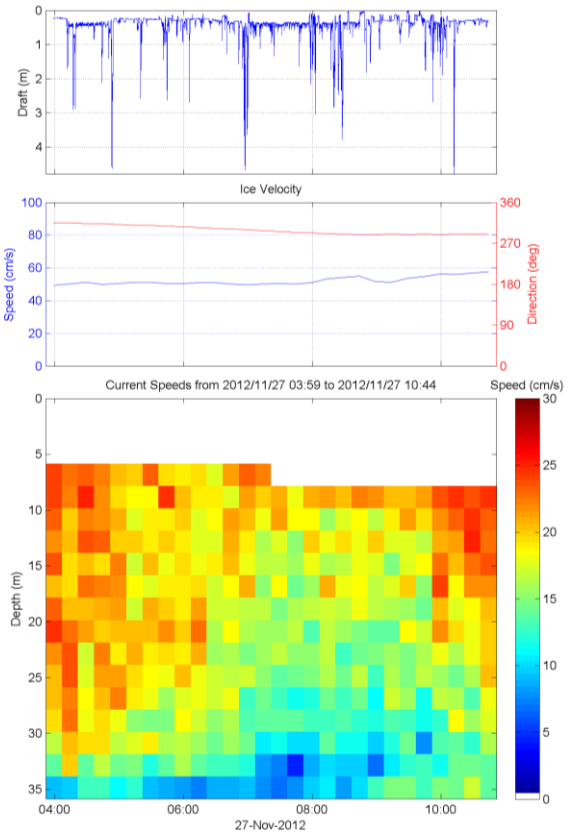

Figure 10. Example of a large ice drift event with stable ice speeds (middle panel) in the Chukchi Sea from November 27, 2012. The concurrent ice drafts are shown in the upper panel, and the concurrent ocean currents are shown in the lower panel.

The currents from the November large drift event were placed in an ice-centric reference frame by subtracting the ice drift velocity from the measured currents. These ice-centric currents were vector averaged into a single profile and logarithmically fitted (Figure 10). The results are a roughness scale of z_o ~ 2.9 cm and a friction velocity of u_* ~ 3.1 cm/s. These numbers are consistent with McPhee (2013), given the moderately deformed ice conditions prevalent at this time of year due to brash ice conditions. McPhee (2013) reported that undeformed ice has a roughness of about 0.1 to 0.6 cm, deformed pack ice has a roughness of about 4 cm, while rough ice in the Beaufort Sea produced a roughness of about 9 cm.

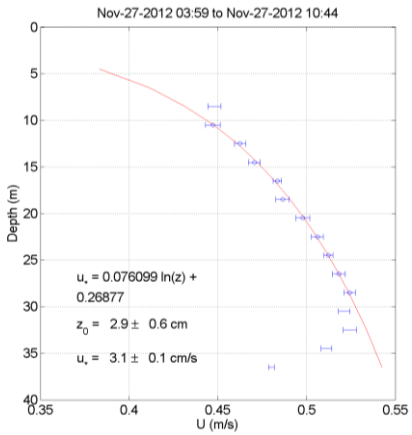

Figure 11. Vector average current speed profile in the ice reference frame from November 27, 2012. The region marked by circles was fitted.

A roughness of 2.9 cm when scaled by 30, as suggested by McPhee (2013) and others, indicates the under ice draft roughness is on the order of 87 cm. The ice in November was relatively thin and with a limited degree of deformation. An estimate for the roughness was made based on the standard deviation of the high pass filtered ice draft spatial series (Figure 12). The standard deviation for this November 27th period is 40 cm .This number is about one half what is estimated by the log layer analysis. Further examples of turbulent logarithmic boundary layers have been explored from the same year of data.

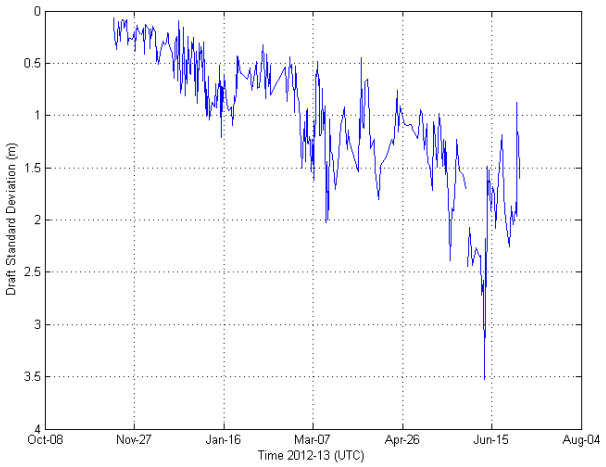

Figure 12. Standard deviation of IPS ice draft. The spatial series was high passed filtered with a 5 point Butterworth filter that had a 300 m spatial cut-off. The filter is run forward and backward through the time-series to eliminate phase shifts. The standard deviations are calculated for 10 km windows.

On January 14, 2013, a period with larger ice velocities but lower current shear was considered (Figure 13 and 14). The log layer analysis provides a z_o ~ 1.6 cm and a friction velocity of u_* ~ 2.5 cm/s. The standard deviation of the ice draft for the period was 76 cm, making for a ratio of 48. The value is reasonable given the error in the roughness is ± 1.2 cm.

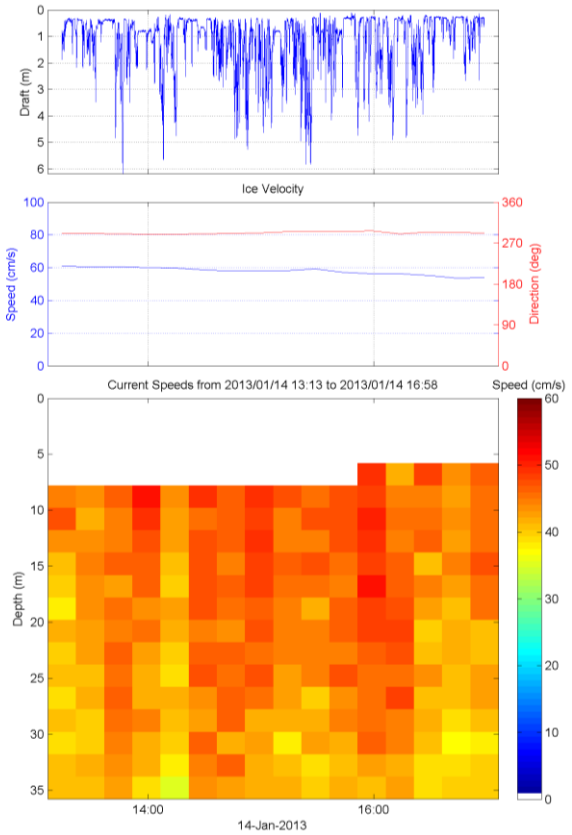

Figure 13. Example of a large ice drift event with stable ice speeds (middle panel) in the Chukchi Sea from January 14, 2013. The concurrent ice drafts are shown in the upper panel, and the concurrent ocean currents are shown in the lower panel.

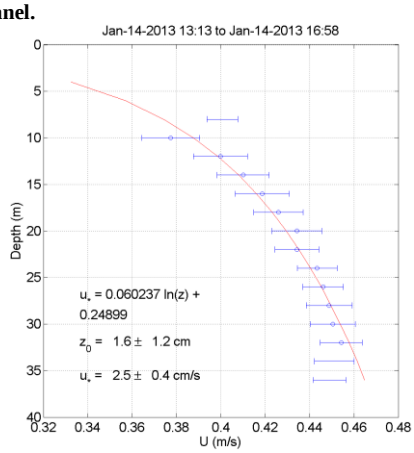

Figure 14. Vector average current speed profile in the ice reference frame from January 14, 2013. The region below 32 m was not fitted as it no longer followed the logarithmic distribution.

On May 9, 2013, a period with weaker ice velocities and high current shear was considered (Figures 15 and 16). The log layer analysis provides a z_o ~ 91 cm and a friction velocity of u_* ~ 2.5 cm/s. The standard deviation of the ice draft for the period was 96 cm, making for a ratio of nearly 1. The z_o value is clearly unreasonable and has a very large uncertainty of ±275 cm. The current profile in Figure 15 is suggestive of the presence of stratification and either the case should be dropped or the modified law-of-the-wall fit should be used.

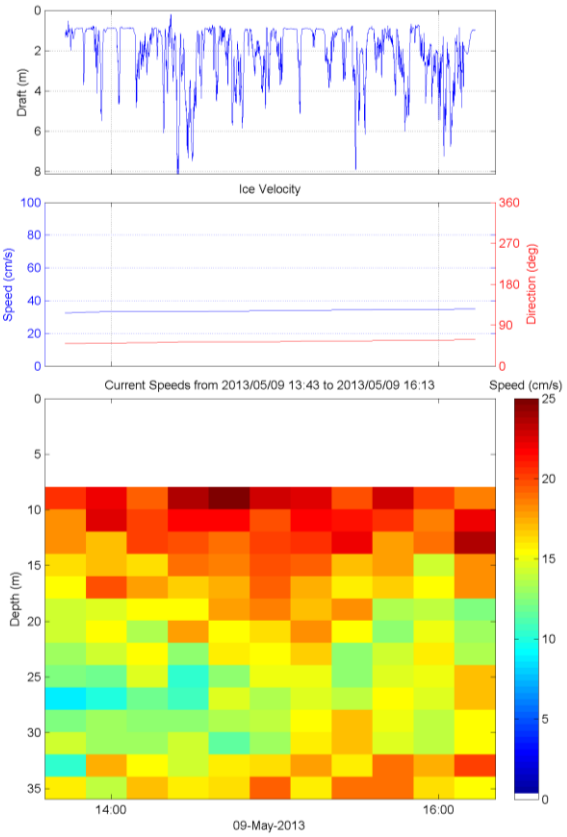

Figure 15. Example of a large ice drift event with stable ice speeds (middle panel) in the Chukchi Sea from May 9, 2013. The concurrent ice drafts are shown in the upper panel, and the concurrent ocean currents are shown in the lower panel.

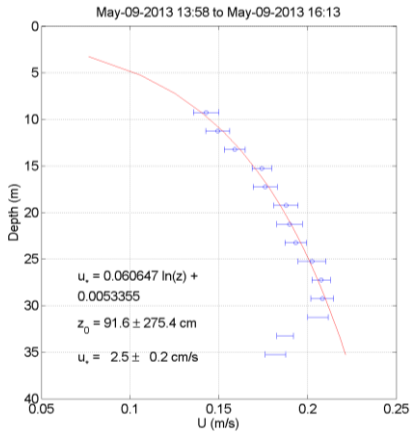

Figure 16. Vector average current speed profile in the ice reference frame from May 9, 2013. The region below 30 m was not fitted as it no longer followed the logarithmic distribution.

A further six examples were considered (Table 1) within the same ice season (2012-2013) at the same site. Of these, two appear to be influenced by stratification with an exceptionally high friction velocity of 5.3 cm/s and roughness of 185 cm for the January 6, 2013 example. The other examples had frictional velocities of 1.8 to 3.4 cm/s and roughness estimates of 0.2 to 11 cm. The relative errors in the friction velocities are small; however, roughness errors are 20% to 100% of the estimates.

Table 1. Tabulation of nine steady ice motion events and the associated roughness length scale (z_0), friction velocity (u_*), standard deviation in the 300m high pass ice draft (σ_{IPS}), median ice draft, log layer depth, mean ice speed, and z_0/ σ_{IPS}.

Start Time	Stop Time	z_o (cm)	u_* (cm/s)	σ_{IPS} (m)	Median Draft (m)	Log Layer Depth (m)	Mean Ice Speed (cm/s)	Ratio σ_{IPS}/z_o
Nov-27-2012 03:59	Nov-27-2012 10:44	2.9 ± 0.6	3.1 ± 0.1	0.40	0.35	29	52	14
Nov-27-2012 14:29	Nov-27-2012 15:59	0.7 ± 0.7	2.5 ± 0.4	0.17	0.35	17	52	24
Dec-21-2012 10:29	Dec-21-2012 19:44	7.8 ± 1.3	3.2 ± 0.1	0.57	0.65	27	56	7.3
Dec-21-2012 16:14	Dec-21-2012 19:59	1.8 ± 0.6	2.6 ± 0.2	0.50	0.62	27	59	28
Dec-21-2012 19:59	Dec-22-2012 01:59	0.2 ± 0.2	1.8 ± 0.3	0.12	0.68	26	59	73
Jan-06-2013 11:59	Jan-06-2013 17:44	184.9 ± 43.5 [x]	5.3 ± 0.3	1.11	0.93	24	34	0.6
Jan-14-2013 10:58	Jan-14-2013 12:58	10.9 ± 2.1	3.4 ± 0.2	0.58	0.67	36	59	5.4
Jan-14-2013 13:13	Jan-14-2013 16:58	1.6 ± 1.2	2.5 ± 0.4	0.76	0.78	32	58	48
May-09-2013 13:58	May-09-2013 16:13	91.6 ±275.4 [xx]	2.5 ± 0.2	0.96	1.68	29	34	1.1

x Jan-06. Not many points near surface. Stratified.
xx May-09. Stratified.

SUMMARY AND CONCLUSIONS

The development of a new algorithm for near surface current measurements provides contiguous high-quality current data from near the ice/sea and air/sea interface. The method reduces the amount of manual editing, including data removal and fitting, that had previously been required. This provides more consistent ocean current data products for inputs into engineering design.

The new methods and products developed for the near-surface bin allows for the development of new data products. The ice/water boundary layer was investigated. Given the inability to resolve the first few metres below the ice due to the depth of the ADCPs in the Chukchi and Beaufort Seas, only cases of high and near constant ice speeds were considered.

Examples from the 2012-2013 ice season provided reasonable results for 7 out of 9 examples that were investigated. Friction velocities ranged from 1.8 to 3.4 cm/s with relatively small error estimates. The turbulent roughness scales, z_o , correspond to those reported by McPhee (2013) for a range of sea ice conditions from undeformed (0.2 cm) to heavily deformed (10 cm). The other examples appeared to be influenced by the presence of turbulence. There is a trend towards larger roughness length scales with the presence of more deformed ice; however, the estimated error in the turbulent roughness scales is quite large (20 to 100%). Further work is required to investigate more cases and confirm the validity of working more than 3 m away from the ice/sea boundary.

ACKNOWLEDGEMENTS

We would like to thank Shell, ConocoPhillips, Statoil and Olgoonik Fairweather for access to the data sets and support for this paper.

REFERENCES

Ekman, V. W. "On the influence of the earth's rotation on ocean currents". Arch.Math. Astron. Phys., 2, 1{52, 1905.

Fissel, D.B., Marko, J.R., Ross, E., Chave, R.A. and J. Egan. "Improvements in upward looking sonar-based sea ice measurements: a case study for 2007 ice features in Northumberland Strait, Canada", in Proceedings of Oceans 2007 Conference, Vancouver, B.C., Canada, 6p. IEEE Press, 2007.

Lueck, R. G., and Lu, Y., "The logarithmic layer in a tidal channel". Cont. Shelf Res. 17, 1785–1801, 1997.

McCave I.N., "Deposition from Suspension", Encyclopedia of Geology: *Sedimentary* Processes, (eds. Selly R.C., Cocks L.R.M., Malone J.M.) Oxford, 5, pp 8-17, 2005.

McPhee, M. G. 2013 "The Ice-Ocean Boundary Layer", submitted as a chapter in Sea Ice, Third Edition, edited by David Thomas

Melling, H., Johnston, P.H. and Reidel, D.L., "Measurements of the Underside Topography of Sea Ice by Moored Subsea Sonar*," J. Atmospheric and Ocean Technology*, 12: 589-602, 1995.

Mudge, T., Sloat, J. and Chen, J. "Discharge and Current Profiles Under the Ice", Proceedings of the IEEE/OES Eighth Working Conference on Current Measurement Technology. 2005.

Perlin, A., J. N. Moum, J. M. Klymak, M. D. Levine, T. Boyd, and P. M. Kosro, "A modified law-of-the-wall applied to oceanic bottom boundary layers", J. Geophys. Res., 110, C10S10, 2005

Tennekes, H., and Lumley, J. L., A first course in turbulence, MIT Press, Cambridge, Mass. 1972.